Conservation of longitudinal spin polarization of positrons emitted from a thin Ni(100) foil

G. G. Cecchini,* R. G. Greaves, and A. P. Mills, Jr.
Department of Physics and Astronomy, University of California Riverside, Riverside, California 92506, USA

(Received 17 December 2022; revised 15 March 2023; accepted 16 May 2023; published 9 June 2023)

We have discovered that 5 keV bursts of 5×10^7 positrons with an initial longitudinal spin polarization of $(28.8 \pm 0.7)\%$, when implanted into a thin Ni(100) crystal, are emitted with 20% efficiency at thermal energies from its surface with $(30.9 \pm 0.5)\%$ polarization. We conclude that the positron spin polarization is preserved while interacting with the Ni, despite the 0.61 T average transverse magnetization of the Ni at room temperature. The resulting polarized beam has been focused to a 0.025-mm mean-diameter spot when accelerated to 5 keV and will be uniquely suited for experiments on a neutral spin aligned e^+-e^- plasma, spin- and angle-resolved positronium emission spectroscopy, and critical for producing a triplet positronium Bose-Einstein condensate.

DOI: 10.1103/PhysRevA.107.062809

I. INTRODUCTION

The spin polarization of an ensemble of positrons is defined as $P = (n_\uparrow - n_\downarrow)/(n_\uparrow + n_\downarrow)$, where $n_{\uparrow,\downarrow}$ are the probabilities of the particles having spins parallel or antiparallel to the axis of quantization. Positrons obtained from the β^+ decay of certain radioactive isotopes (^{22}Na, ^{64}Cu, etc.) are naturally produced with a helicity equal to the emission velocity divided by the speed of light [1]. By selecting a limited solid angle of the emitted positrons, a distribution of partially spin-polarized energetic positrons is obtained that may be implanted directly into a sample to measure the spin-polarized angular distribution of the annihilation radiation [2–4]. Energetic polarized positrons may also be moderated [5,6] (i.e., implanted into a surface such as solid Ne from which up to 1% of the positrons emerge at 1 eV energies) and remoderated [7,8] (i.e., accelerated to ∼5 keV and focused to a small spot on a second moderator) to obtain bright beams that can be electrostatically focused while retaining their direction of spin polarization [9–11]. Such beams [12,13] can be used for angle- [14] and spin- [15,16] resolved positronium emission spectroscopy at the surface of devices operating *in situ* and for observing edge states in materials such as Weyl semimetals [17]. They [18] may also be trapped and accumulated to produce nanosecond positron bursts useful for (1) making confined collections of millions of polarized positrons plus neutralizing electrons for studying relatively low-density (10^{10}–10^{14} cm^{-3}) pure electron-positron plasmas [19,20], (2) probing the spin polarization of outermost surface electrons [21,22], and (3) for producing high-density (more than 10^{18} cm^{-3}) collections of cold spin-polarized Ps atoms for producing a Ps Bose-Einstein condensate (BEC) [23] and observing the stimulated emission of two-photon annihilation radiation [24].

In a scenario [25] for producing a BEC of positronium atoms (Ps) every parameter is at the limit of what is currently possible. In particular, a thin Ni(100) crystal would be the best remoderator for this experiment. However, Ni has an average internal transverse magnetic field of 0.616 ± 0.002 T at 293 K [26], and there was uncertainty about whether positron spin precession about the transverse micron scale internal magnetic fields [27] would depolarize the positrons and so prevent attainment of the necessary density of polarized positronium in a microscopic cavity. To see if we will be able to make use of the otherwise good qualities of Ni we have directly measured the longitudinal polarization of a positron beam both before and after being remoderated in a Ni(100) film.

The remoderator, a single-crystal Ni(100) film 150 nm thick and of 3 mm diameter [28], was prepared via *in situ* heating with a tungsten halogen lamp [29] and had a 20% slow positron reemission efficiency for 5 keV positrons and a narrow spread of emission energies [30–32]. The next best alternative, tungsten, has a comparable total slow positron yield, but the slow positron energy spread is more than twice that of Ni [33], which would increase the final focused spot size beyond the critical value needed for our intended experiments. Experiments show that thermal energy muons implanted with their velocities perpendicular to the internal magnetic field of a Ni target experience precession about an average internal field $B_\mu = 0.15$ T [34]. Since positrons and positive muons are both light positive quantum particles, they would be expected not to form positronium or muonium in the high-density electron gas. They would also be similar in avoiding the Ni ions and being mostly confined in the centers of the Ni fcc unit cells. Most of the magnetic field in the crystal can be attributed to Ni atomic dipoles. A model calculation using point dipoles at the fcc atom locations predicts zero magnetic field at the centers of the unit cells. This explains the small value of the average internal field B_μ sampled by muons and suggests an analogous result would hold for positrons. The measurements described herein indeed show that the polarization of a Ni-remoderated positron beam is approximately the same as that of the incoming beam.

II. EXPERIMENT

For our experiment, positrons from a 20 mCi ^{22}Na sealed source [35] are moderated to 1–2 eV energies with solid

*Gcecc001@ucr.edu

 ©2023 American Physical Society

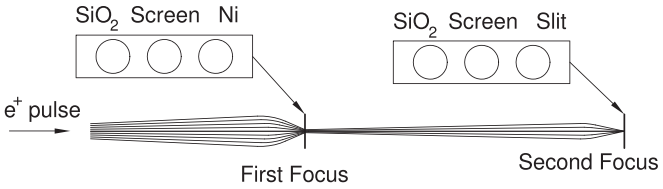

FIG. 1. Layout of electrostatic focus and sample slides. Lens elements have been omitted for clarity. The slides include identically prepared porous silica targets (SiO_2), P-22 phosphor screens, a 150-nm-thick Ni foil, annealed *in situ*, and a 120-μm narrow transmitting slit.

Ne [36] with 0.4% efficiency and captured in a Surko-type Penning-Malmberg trap [37,38] producing pulses of 1×10^5 positrons at a rate of 2 Hz. The pulses are magnetically transported to a UHV positron accumulator [39] where about 500 pulses are collected to produce bursts of 5×10^7 positrons that are compressed to a dense plasma. The positrons are then ejected from the accumulator and guided by a ∼0.01 T field to a pulsed accelerator which produces a 5 keV, ∼5 ns positron burst. The positrons are extracted from the guiding magnetic field [40] and drift to a magnetic-field-free ($B \lesssim 5 \times 10^{-7}$ T) electrostatic focusing region where the positron bursts are implanted in a 0.15-mm full width at half maximum (FWHM) diameter spot in a Ni(100) foil at the first focus indicated in Fig. 1.

To measure the polarization, positrons emitted from the transmission side of the Ni foil are accelerated to 5 keV and focused onto the porous silica target [41] at the second focus. About 60% of the positrons annihilate directly with the electrons of the silica target and the remaining 40% form positronium (Ps) [42] by capturing electrons from the target. The singlet and triplet Ps substates annihilate with a 125 ps and ∼70 ns mean lifetime, respectively, with the latter reduced from the 142 ns vacuum lifetime due to collisions with the atoms of the porous sample. Dipositronium formation [43] and spin-exchange collisions quench [44] the triplet population at a density-dependent rate. The positron polarization is deduced from the density dependence of the delayed fraction (f_d) of the long-lived Ps in the annihilation time spectrum [45]. However, whereas a 2.3 T field was used in the Cassidy measurement, the Ps produced in the present experiment is in a magnetic-field-free environment and as such, the analysis differs from Cassidy *et al.* by accounting for (1) the production of $m = 0$ Ps and the contamination of the long-lived Ps signal resulting therefrom, (2) the angular distribution of the three photon annihilation gamma rays, (3) the finite size of the gamma-ray detector, and (4) slight differences in the shapes of the $|m| = 1$ and $m = 0$ gamma-ray energy spectra.

III. MEASUREMENT AND ANALYSIS

Positron annihilations are detected by a single 2.54-cm-diameter $PbWO_4$ scintillation crystal coupled to a Hamamatsu R1924A photomultiplier tube positioned ∼90° from the beam axis with the front face of the scintillation crystal 10 cm away and facing the Ps target. The response of the detector to the 5 ns FWHM, 5 keV positron beam pulse, composed of prompt positron annihilations and singlet Ps decays producing

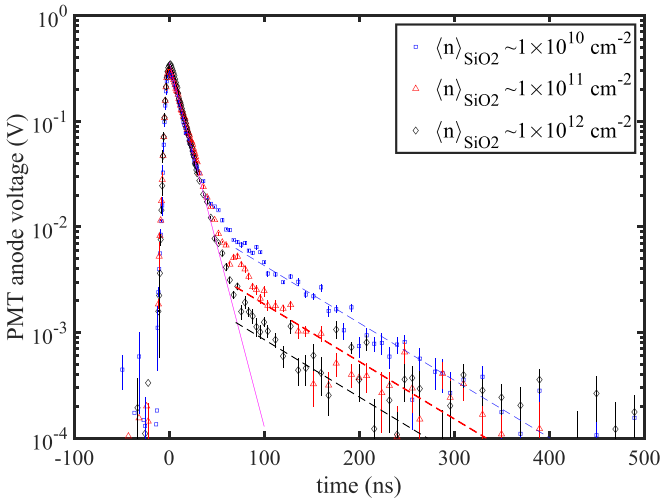

FIG. 2. Annihilation gamma-ray spectra detected using a 2.54 cm diameter×2.54 cm long $PbWO_4$ scintillator coupled to a Hamamatsu R1924A photomultiplier tube. Spectra are a result of implanting 5 keV positrons into a silica target at three different densities. Fits (solid lines) and guides to the eye (dashed lines) for the prompt signal and the delayed signals have been added. The guides to the eye have been included here only to illustrate the reduced delayed signal as a consequence of increasing the density of impinging positrons since the delayed fraction method described in the text does not require fitting routines. Here, the density-weighted areal density $\langle n \rangle$ is used.

pairs of antiparallel 511 keV photons, is a large-amplitude prompt pulse from about 10^5 detected gamma rays with a 12.6 ns decay time characteristic of the $PbWO_4$ scintillator, and is shown along with a fit in Fig. 2. Triplet Ps atoms with magnetic quantum numbers $m = +1$, 0, and -1 decay into two or three coplanar photons with total energy 1022 keV and an approximately exponentially decaying signal with a ∼70 ns lifetime from pick-off annihilations. A third decay component at the juncture between the 12.6- and 70-ns components is from $m = 0/m = 0$ and $m = +1/m = -1$ triplet Ps collisions with a decay rate that varies with the Ps density.

The delayed fraction (f_d), employed here to calculate the positron polarization, is defined as the sum of the spectral counts starting at a time $t_1 > 0$ where only the long-lived $|m| = 1$ annihilation component is significant, up to $t_2 = +300$ ns, divided by the sum over the spectrum in the range from -50 ns to t_2. Thus the delayed fraction f_d is proportional to the number (n) of long lived o-Ps atoms. The plot of f_d recorded versus t_1, displayed in the inset within Fig. 3, shows that as t_1 increases, f_d at first decreases and then becomes a constant. While Cassidy *et al.* used $t_1 = 50$ ns, in our experiment we require $t_1 > 75$ ns so that f_d has essentially no contamination from either the rapidly decaying prompt component or the self-quenched intermediate component. The positron areal density-weighted density, hereafter referred to simply as density and denoted as $\langle n \rangle$, is varied over a wide range by adjusting the voltages on the electrostatic lenses. The annihilation lifetime curves shown in Fig. 2 were obtained at the second focus, with $\langle n \rangle_{SiO_2} \approx 10^{10}$, 10^{11}, and 10^{12} cm^{-2}, the densities being separately measured with the phosphor

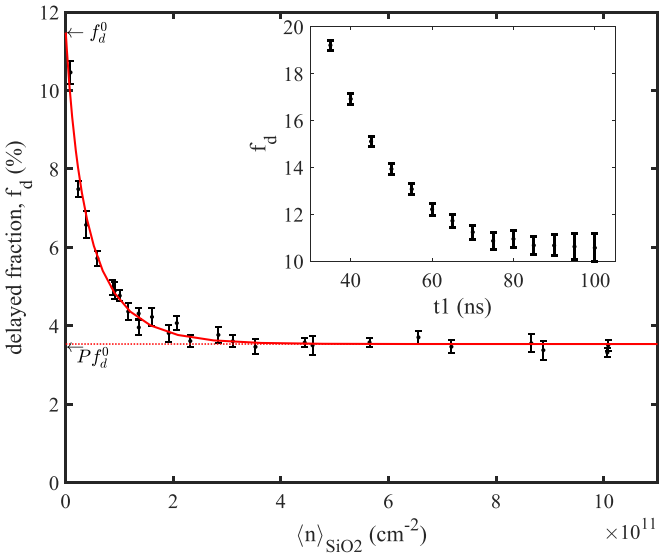

FIG. 3. A sample polarization measurement resulting from positrons being densely implanted in a thin 150-nm Ni foil, extracted from the transmission side of the foil, and then implanted into a silica target. The positron implantation density in the silica is varied, the delayed fraction is measured, and the result is fitted to Eq. (7), with a y intercept f_d^0, and asymptote Pf_d^0. Inset: The calculated delayed fraction f_d as a function of t_1 as described in the text.

screen and transmitting narrow slit (see Fig. 1), also at the second focus. The beam has a Gaussian profile with a 25 μm FWHM as measured by the phosphor screen, which was purchased from Kimball Physics and had a specified grain size of ∼6 μm, and recorded by an Atik 460 Ex CCD camera with an overall resolution (lenses included) of ∼5 μm. With a 120-μm transmitting slit the beam diameter is measured. We use the phosphor screen to measure the two-dimensional (2D) areal profile of the beam, and the transmitting slit to more accurately measure the beam FWHM.

The quenching effect (Q) that tells us the polarization $P = (n_\uparrow - n_\downarrow)/(n_\uparrow + n_\downarrow)$ of the original positron beam from which the Ps was formed, is the ratio of the delayed fraction f_d^0 extrapolated to very high and very low positron densities as in Fig. 3. The quenching effect Q observed by Cassidy *et al.* [45] was a direct polarization measurement because the long-lived $m = 0$ component was not present, since it was rapidly quenched in the constant 2.3 T magnetic field of that experiment. The quantity that is available experimentally here is the limiting ratio of high versus low f_d that includes the $m = 0$ component at low densities because of the absence of a magnetic field. The measured quenching effect for a 4π detector geometry is then

$$Q = \frac{f_d(^3S_{1,+1}) - f_d(^3S_{1,-1})}{f_d(^3S_{1,+1}) + f_d(^3S_{1,-1}) + f_d(^3S_{1,0})}, \tag{1}$$

where $f_d(^3S_{1,m})$ denote the individual spin components of the delayed fraction components for the sublevels with $m = +1$, 0, and -1, respectively, and

$$f_d(^3S_{1,+1}) + f_d(^3S_{1,-1}) = 2f_d(^3S_{1,0}). \tag{2}$$

The desired quantity is the polarization

$$P = \frac{f_d(^3S_{1,+1}) - f_d(^3S_{1,-1})}{f_d(^3S_{1,+1}) + f_d(^3S_{1,-1})}, \tag{3}$$

which can be written in terms of the measured quantity Q as

$$P = Q\frac{f_d(^3S_{1,+1}) + f_d(^3S_{1,-1}) + f_d(^3S_{1,0})}{f_d(^3S_{1,+1}) + f_d(^3S_{1,-1})}. \tag{4}$$

Using Eq. (2) the polarization of the incoming positron beam calculated from Eq. (4) is then

$$P = Q\frac{2f_d(^3S_{1,0}) + f_d(^3S_{1,0})}{2f_d(^3S_{1,0})} = 1.5\,Q. \tag{5}$$

If the annihilation gamma-ray detector does not have a 4π geometry, there is a geometrical correction that needs to be made to account for the angular distribution of the triplet 3-gamma annihilation photons. According to Drisko [46], the actual counting rates for a small-diameter single detector perpendicular to the polarization axis, are such that if the detection efficiency for $m = +1$ or $m = -1$ is 1, then the detection efficiency for $m = 0$ is 1.357. To find the correct polarization for our detector geometry, we must therefore change the quantity $f_d(^3S_{1,0})$ in Eq. (4) by dividing it by 1.357. For this geometry Eq. (5) is then properly written

$$P = 1.369\,Q. \tag{6}$$

Not included are corrections for the slight differences in the shapes of the $m = 1$ and $m = 0$ gamma-ray energy spectra [47]. From examination of the data of Fig. 2, we find the resulting difference in the total number of delayed counts is less than 1% for spectra containing $m = 0, \pm 1$ versus only $m = +1$ delayed counts. Therefore neglecting the spectral shape differences likely introduces a constant systematic error $|\Delta P| = 0.01P$. It is important to repeat that the Cassidy experiment was carried out totally in a 2.3 T magnetic field, so that the triplet $m = 0$ Ps is always quenched and the spectral corrections just mentioned do not apply.

The functional relationship between the normalized amplitude of the delayed fraction, $a(\zeta n)$, and positron implantation density are defined by Cassidy *et al.* [45] as

$$a(\zeta n) = f_d^0 P\big[1 + P\tanh\big\{\tfrac{1}{2}P\zeta n\big\}\big]\big/\big[P + \tanh\big\{\tfrac{1}{2}P\zeta n\big\}\big]. \tag{7}$$

Here, (1) a normalizing factor f_d^0 has been included, (2) the symbol for the polarization P has replaced the p_0 of Cassidy *et al.*, and (3) ζ is an independent fitting parameter. The density n is varied via the focus voltage and increased just beyond the maximum density value found with the phosphor screen in place in order to correct for slight changes in the electrostatic configuration between the phosphor screen and the silica target. We find the focus voltage settings for the minimum spot size and delayed fraction differ by about 5%. With that corrected for, the delayed fraction as a function of implantation density (shown in Fig. 3), is found from a fit to Eq. (7). This is repeated for several implantation densities at the Ni foil. Lower densities at the Ni foil result in lower maximum densities at the silica target, which may lead to spuriously low polarization estimates from the fitting routine. As such, several measurements are made where the maximum

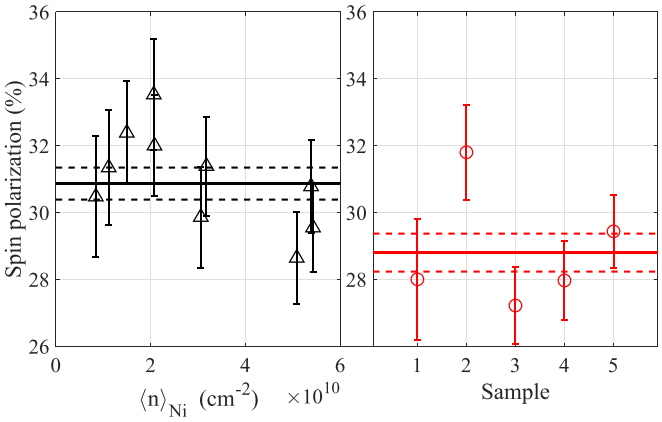

FIG. 4. Left panel: Polarization of positrons emitted from a thin Ni(100) crystal as a function of implanted positron density. The density ($\langle n \rangle_{\mathrm{Ni}}$) reported here is measured using a phosphor screen at the same location. Right panel: Five measurements of the positron polarization before remoderation. The solid horizontal lines are the weighted means and the dashed lines are the standard errors of the mean positron spin polarizations. Not shown is an estimated ±1% systematic scale error common in both measurements.

density at the silica target is sufficiently high to adequately constrain the asymptotic behavior of the fit function [Eq. (7)], such as that shown in Fig. 3. The fit parameters ζ and f_d^0 are then fixed, and the data reanalyzed with the only free parameter being the polarization.

IV. RESULTS

The result, shown in the left panel of Fig. 4, is a positron spin polarization of $(30.9 \pm 0.5)\%$, independent of the density of positrons impinging on the Ni foil. There is no evidence that the density of positron surface states [48] on the transmission side of the Ni foil or in the bulk was sufficient to increase the reemitted positron spin polarization via the destruction of minority-spin positrons. Replacing the Ni foil with a silica target at the first focus, and employing the same techniques described above, we display in the right panel of Fig. 4 five measurements of the positron spin polarization prior to remoderation, for which the mean value is $(28.8 \pm 0.7)\%$. Although the two polarization measurements differ by 2.4 σ's, better statistics would be required to confirm an actual difference in polarization. There is also no evidence for spin depolarization due to the precession of positron spins within the Ni foil.

The reader will note that the polarization reported here is slightly higher (31% vs 28%) than that of Cassidy *et al.* [45]. This might not be significant since there could be small manufacturing variations in the self-attenuation of the primary positron sources which might lead to changes of this magnitude in the slow positron spin polarization [18].

V. CONCLUSION

The experiments described herein prove that the polarization is in fact essentially unchanged upon implantation and reemission of thermal positrons from a 150-nm-thin crystal of ferromagnetic Ni(100) at room temperature. The effective average transverse magnetic field sampled by positrons in the foil is at least 5× less than the average spatial magnetization. This establishes Ni(100), with its narrow reemitted positron energy spread and high positron yield, as an ideal single-crystal remoderator for obtaining high brightness positron beams for the many applications where high spin polarization is critical. Foremost among these are the effort to produce a Ps BEC, the further development of spin- and angle-resolved Ps emission spectroscopy, the probing of surface spin states on metals [22], and resolving spin textures associated with topological states in topological insulators [49].

ACKNOWLEDGMENTS

This work was supported in part by the National Science Foundation under Grant No. 2011836, and by a National Science Foundation MPS-Ascend Post-doctoral Research Fellowship under Grant No. 2213812.

[1] J. D. Jackson, S. B. Treiman, and H. W. Wyld, Jr., Possible tests of time reversal invariance in beta decay, Phys. Rev. **106**, 517 (1957).
[2] S. S. Hanna and R. S. Preston, Positron polarization demonstrated by annihilation in magnetised iron, Phys. Rev. **106**, 1363 (1957).
[3] P. E. Mijnarends and L. Hambro, Positron annihilation in magnetised single crystals of iron, Phys. Lett. **10**, 272 (1964).
[4] S. Berko and J. Zuckerman, Polarized Positron Annihilation in Ferromagnets, Phys. Rev. Lett. **13**, 339 (1964).
[5] W. H. Cherry, Secondary electron emission produced from surfaces by positron bombardment, Ph.D. thesis, Princeton University, 1958.
[6] K. F. Canter, P. G. Coleman, T. C. Griffith, and G. R. Heyland, Measurement of total cross sections for low energy positron-helium collisions, J. Phys. B: At., Mol. Phys. **5**, L167 (1972).
[7] A. P. Mills, Jr., Brightness enhancement of slow positron beams, Appl. Phys. **23**, 189 (1980).
[8] P. J. Schultz, E. M. Gullikson, and A. P. Mills, Jr., Transmitted positron reemission from a thin single-crystal Ni (100) foil, Phys. Rev. B **34**, 442 (1986).
[9] P. W. Zitzewitz, J. C. Van House, A. Rich, and D. W. Gidley, Spin Polarization of Low-Energy Positron Beams, Phys. Rev. Lett. **43**, 1281 (1979).
[10] D. W. Gidley, A. R. Köymen, and T. W. Capehart, Polarized Low-Energy Positrons: A New Probe of Surface Magnetism, Phys. Rev. Lett. **49**, 1779 (1982).
[11] J. Van House and P. W. Zitzewitz, Probing the positron moderation process using high-intensity, highly polarized slow-positron beams, Phys. Rev. A **29**, 96 (1984).
[12] J. Van House and A. Rich, Surface Investigations Using the Positron Reemission Microscope, Phys. Rev. Lett. **61**, 488 (1988).

[13] G. R. Brandes, K. F. Canter, and A. P. Mills, Jr., Sub-Micron Resolution Study of a Thin Ni Crystal Using a Brightness-Enhanced Positron Reemission Microscope, Phys. Rev. Lett. **61**, 492 (1988).

[14] A. C. L. Jones, H. J. Rutbeck-Goldman, T. H. Hisakado, A. M. Piñeiro, H. W. K. Tom, A. P. Mills, Jr., B. Barbiellini, and J. Kuriplach, Angle-Resolved Spectroscopy of Positronium Emission from a Cu(110) Surface, Phys. Rev. Lett. **117**, 216402 (2016).

[15] M. Maekawa, H. Abe, A. Miyashita, S. Sakai, S. Yamamoto, and S. Kawasuso, Vacancy-induced ferromagnetism in ZnO probed by spin-polarized positron annihilation spectroscopy, Appl. Phys. Lett. **110**, 172402 (2017).

[16] M. Maekawa, A. Miyashita, S. Sakai, S. Li, S. Entani, A. Kawasuso, and Y. Sakuraba, Spin-Polarized Positronium Time-of-Flight Spectroscopy for Probing Spin-Polarized Surface Electronic States, Phys. Rev. Lett. **126**, 186401 (2021).

[17] N. P. Armitage, E. J. Mele, and A. Vishwanath, Weyl and Dirac semimetals in three-dimensional solids, Rev. Mod. Phys. **90**, 015001 (2018).

[18] A. Rich, R. S. Conti, D. W. Gidley, M. Skalsey, J. Van House, and P. W. Zitzewitz, Production and applications of monoenergetic polarized positron beams, Hyperfine Interact. **44**, 125 (1989).

[19] V. Tsytovich and C. B. Wharton, Laboratory electron-positron plasma — a new research object, Comments Plasma Phys. Controlled Fusion **4**, 91 (1978).

[20] R. G. Greaves and C. M. Surko, An Electron-Positron Beam-Plasma Experiment, Phys. Rev. Lett. **75**, 3846 (1995).

[21] H. J. Zhang, S. Yamamoto, B. Gu, H. Li, M. Maekawa, Y. Fukaya, and A. Kawasuso, Charge-to-Spin Conversion and Spin Diffusion in Bi/Ag Bilayers Observed by Spin-Polarized Positron Beam, Phys. Rev. Lett. **114**, 166602 (2015).

[22] H. J. Zhang, S. Yamamoto, Y. Fukaya, M. Maekawa, H. Li, A. Kawasuso, T. Seki, E. Saitoh, and K. Takanashi, Current-induced spin polarization on metal surfaces probed by spin-polarized positron beam, Sci. Rep. **4**, 4844 (2014).

[23] P. M. Platzman and A. P. Mills, Jr., Possibilities for Bose condensation of positronium, Phys. Rev. B **49**, 454 (1994).

[24] H. K. Avetissian, A. K. Avetissian, and G. F. Mkrtchian, Gamma-ray laser based on the collective decay of positronium atoms in a Bose-Einstein condensate, Phys. Rev. A **92**, 023820 (2015).

[25] M. X. Asaro, S. Herrera, M. Fuentes-Garcia, G. G. Cecchini, E. E. Membreno, R. G. Greaves, and A. P. Mills, Jr., Conditions for obtaining positronium Bose–Einstein condensation in a micron-sized cavity, Eur. Phys. J. D **76**, 107 (2022).

[26] C. D. Graham, Jr., Iron and nickel as magnetization standards, J. Appl. Phys. **53**, 2032 (1982).

[27] R. W. De Blois, Ferromagnetic domains in thin single-crystal nickel platelets, J. Appl. Phys. **36**, 1647 (1965).

[28] The Ni(100) samples were obtained from Bine Hansen, Aarhus University, Institut for Physics and Astronomi, Building 1520, Ny Munkegade 120, 8000 Aarhus C, Denmark.

[29] A. G. Krupyshev, Diamond and Si (100)(1 × 1)-2H surface structure determination by LEPD, Ph.D. thesis, Brandeis University, 2000, available from University Microfilms.

[30] W. E. Frieze, D. W. Gidley, and K. G. Lynn, Positron-beam-brightness enhancement: Low-energy positron diffraction and other applications, Phys. Rev. B **31**, 5628 (1985).

[31] F. M. Jacobsen, M. Petkov, and K. G. Lynn, Electric-field-assisted moderator for generation of intense low-energy positron beams, Phys. Rev. B **57**, 6998 (1998).

[32] A. Zecca, L. Chiari, A. Sarkar, S. Chattopadhyay, and M. Brunger, Procedures for conditioning W- and Ni-moderators for application in positron-scattering measurements, Nucl. Instrum. Methods Phys. Res., Sect. B **268**, 533 (2010).

[33] D. M. Chen, K. G. Lynn, R. Pareja, and B. Nielsen, Measurement of positron reemission from thin single-crystal W(100) films, Phys. Rev. B **31**, 4123 (1985).

[34] M. Foy, N. Heiman, W. Kossler, and C. Stronach, Precession of Positive Muons in Nickel and Iron, Phys. Rev. Lett. **30**, 1064 (1973).

[35] Source procured from iThemba Labs, South Africa.

[36] A. P. Mills, Jr. and E. M. Gullikson, Solid neon moderator for producing slow positrons, Appl. Phys. Lett. **49**, 1121 (1986).

[37] C. M. Surko and R. G. Greaves, Emerging science and technology of antimatter plasmas and trap-based beams, Phys. Plasmas **11**, 2333 (2004).

[38] R. G. Greaves and J. M. Moxom, Compression of trapped positrons in a single particle regime by a rotating electric field, Phys. Plasmas **15**, 072304 (2008).

[39] D. B. Cassidy, S. H. M. Deng, R. G. Greaves, and A. P. Mills, Jr., Accumulator for the production of intense positron pulses, Rev. Sci. Instrum. **77**, 073106 (2006).

[40] N. C. Hurst, J. R. Danielson, and C. M. Surko, Magnetic field extraction of trap-based electron beams using a high-permeability grid, Phys. Plasmas **22**, 073503 (2015).

[41] The Ps producing silica targets are produced from tetraethyl orthosilicate (TEOS) mixed with porogen (P-127) and spin coated onto a Si wafer. The sample is then calcined into a porous thin film in a tube furnace. A 30-nm layer of dense SiO_2 is sputter coated to reflect positrons back into the TEOS and 10 nm of aluminum is sputter coated to make a front facing grounding plane, reducing charging of the surface upon positron implantation.

[42] D. B. Cassidy, T. H. Hisakado, V. E. Meligne, H. W. K. Tom, and A. P. Mills, Delayed emission of cold positronium from mesoporous materials, Phys. Rev. A **82**, 052511 (2010).

[43] D. B. Cassidy and A. P. Mills, Jr., The production of molecular positronium, Nature (London) **449**, 195 (2007).

[44] R. A. Ferrell, Ortho-parapositronium quenching by paramagnetic molecules and ions, Phys. Rev. **110**, 1355 (1958).

[45] D. B. Cassidy, V. E. Meligne, and A. P. Mills, Jr., Production of a Fully Spin-Polarized Ensemble of Positronium Atoms, Phys. Rev. Lett. **104**, 173401 (2010).

[46] R. M. Drisko, Spin and polarization effects in the annihilation of triplet positronium, Phys. Rev. **102**, 1542 (1956).

[47] The shapes also happen to depend on the angle of the detector with respect to the beam axis.

[48] A. P. Mills, Jr., Possible experiments with high density positronium, in *The 18th International Conference on Positron Annihilation (ICPA-18), Florida, USA*, edited by F. Selim, AIP Conf. Proc. Vol. 2182 (AIP Publishing, Melville, NY, 2019), p. 030001.

[49] V. Callewaert, K. Shastry, R. Saniz, I. Makkonen, B. Barbiellini, B. A. Assaf, D. Heiman, J. S. Moodera, B. Partoens, A. Bansil, and A. H. Weiss, Positron surface state as a spectroscopic probe for characterizing surfaces of topological insulator materials, Phys. Rev. B **94**, 115411 (2016).